Arabidopsis INOSITOL TRANSPORTER2 Mediates H^+ Symport of Different Inositol Epimers and Derivatives across the Plasma Membrane[1][C][OA]

Sabine Schneider, Alexander Schneidereit, Patrick Udvardi, Ulrich Hammes, Monika Gramann, Petra Dietrich, and Norbert Sauer*

Molekulare Pflanzenphysiologie, Friedrich-Alexander-Universität Erlangen-Nürnberg, D–91058 Erlangen, Germany

Of the four genes of the Arabidopsis (*Arabidopsis thaliana*) *INOSITOL TRANSPORTER* family (*AtINT* family) so far only *AtINT4* has been described. Here we present the characterization of *AtINT2* and *AtINT3*. cDNA sequencing revealed that the *AtINT3* gene is incorrectly spliced and encodes a truncated protein of only 182 amino acids with four transmembrane helices. In contrast, *AtINT2* codes for a functional transporter. AtINT2 localization in the plasma membrane was demonstrated by transient expression of an *AtINT2-GREEN FLUORESCENT PROTEIN* fusion in Arabidopsis and tobacco (*Nicotiana tabacum*) epidermis cells and in Arabidopsis protoplasts. Its functional and kinetic properties were determined by expression in yeast (*Saccharomyces cerevisiae*) cells and *Xenopus laevis* oocytes. Expression of *AtINT2* in a Δitr1 (inositol uptake)/Δino1 (inositol biosynthesis) double mutant of bakers' yeast complemented the deficiency of this mutant to grow on low concentrations of myoinositol. In oocytes, AtINT2 mediated the symport of H^+ and several inositol epimers, such as myoinositol, scylloinositol, D-chiroinositol, and mucoinositol. The preference for individual epimers differed from that found for AtINT4. Moreover, AtINT2 has a lower affinity for myoinositol (K_m = 0.7–1.0 mM) than AtINT4 (K_m = 0.24 mM), and the K_m is slightly voltage dependent, which was not observed for AtINT4. Organ and tissue specificity of *AtINT2* expression was analyzed in *AtINT2* promoter/reporter gene plants and showed weak expression in the anther tapetum, the vasculature, and the leaf mesophyll. A T-DNA insertion line (Atint2.1) and an *Atint2.1/Atint4.2* double mutant were analyzed under different growth conditions. The physiological roles of AtINT2 are discussed.

Myoinositol and its derivatives are central to numerous metabolic pathways under different physiological conditions. Myoinositol is a precursor in the biosynthesis of UDP-GlcUA, GalUA, Xyl, apiose, and Ara (Loewus and Murthy, 2000; Kanter et al., 2005), it is used for the formation of galactinol, a myoinositol-linked, activated form of Gal that is used for the biosynthesis of raffinose and its derivatives (Kandler and Hopf, 1982), and it is thought to be an initial substrate in the biosynthesis of L-ascorbic acid (Lorence et al., 2004). It may be conjugated to auxins to prevent their biological activity and to allow long-distance transport (Cohen and Bandurski, 1982), and in phospholipids (Lehle, 1990) or glycosylphosphatidylinositol-membrane anchors (Schultz et al., 1998) myoinositol provides the structural basis for membranes and membrane-attached proteins. Inositol-1,4,5-triphosphate plays an important role as second messenger, and myoinositol-1,2,3,4,5,6-hexakisphosphate (phytate) is used for the storage of inositol, phosphorus, and minerals (Shi et al., 2005), or as a structural component of proteins (Macbeth et al., 2005; Tan et al., 2007). Finally, myoinositol may represent a cellular energy currency (Raboy, 2003).

Living cells possess different inositol epimers, the most frequent ones being scylloinositol and D- or L-chiroinositol, and all of these epimers are found in phosphatidyl inositols (Narasimhan et al., 1997). Moreover, monomethylated inositols are found in all plants but are especially common in legumes. In leaves of unstressed soybean (*Glycine max*), for example, concentrations of pinitol (3-*O*-methyl-chiroinositol) can be 2-fold higher than the combined concentrations of Suc, all monosaccharides, and myoinositol (Smith and Phillips, 1982; Streeter et al., 2001). This already high concentration is further increased in drought-stressed plants, underlining the important role of unmethylated and methylated inositols as osmoprotectants (Thomas and Bohnert, 1993; Sheveleva et al., 1997; Nelson et al., 1998; Hasegawa et al., 2000; Streeter et al., 2001; Murakeözy et al., 2003).

The first cDNAs of putative plant myoinositol transporters, MITR1 and MITR2, were cloned from ice

[1] This work was supported by a grant from the Deutsche Forschungsgemeinschaft (Arabidopsis Functional Genomics Network; grant no. Sa 382/13–1 to N.S.).

* Corresponding author; e-mail nsauer@biologie.uni-erlangen.de.

The author responsible for distribution of materials integral to the findings presented in this article in accordance with the policy described in the Instructions for Authors (www.plantphysiol.org) is: Norbert Sauer (nsauer@biologie.uni-erlangen.de).

[C] Some figures in this article are displayed in color online but in black and white in the print edition.

[OA] Open Access articles can be viewed online without a subscription.

www.plantphysiol.org/cgi/doi/10.1104/pp.107.109033

plants (*Mesembryanthemum crystallinum*), and *MITR1*-expressing yeast (*Saccharomyces cerevisiae*) cells were able to grow on lower extracellular concentrations of myoinositol than control cells (Chauhan et al., 2000). Only recently, Schneider et al. (2006) published a detailed functional characterization of the Arabidopsis (*Arabidopsis thaliana*) myoinositol transporter AtINT4 (At4g16480). This protein was characterized as a high-affinity, energy-dependent, plasma membrane-localized H^+/inositol symporter.

Here we present the molecular cloning of an *AtINT2* cDNA (*At1g30220*), analyses of the tissue-specific expression of the *AtINT2* gene, and the functional characterization and subcellular localization of the AtINT2 protein. Like AtINT4, AtINT2 is a plasma membrane-localized H^+/inositol symporter. Expression of an *AtINT2* cDNA in yeast and in *Xenopus* oocytes, however, revealed significant differences between the kinetic properties and substrate specificities of these transporters. Moreover, analyses of *AtINT2* promoter/*GUS* and *AtINT2* promoter/*GFP* reporter lines showed an expression pattern that differed from that of *AtINT4*. Finally, *Atint2* mutant lines were studied. The putative physiological roles of AtINT2 are discussed.

RESULTS

Cloning of *AtINT2* and *AtINT3* cDNAs

The *AtINT3* gene (*At2g35740*) is predicted to encode a protein of 580 amino acids (NP_181117) that is similar to AtINT2 and AtINT4 with 60.4% and 63.4% identical amino acids, respectively. However, we did not succeed in amplifying an *AtINT3* cDNA by reverse transcription (RT)-PCR. To overcome this problem we generated *AtINT3* overexpressing plant material by infiltration of tobacco (*Nicotiana tabacum*) leaves with an *Agrobacterium tumefaciens* strain carrying the plasmid pPU6. The same strain was used for stable transformation of Arabidopsis. pPU6 drives expression of a genomic *AtINT3* sequence (from start to stop including two predicted introns) under the control of the *35S* promoter. RT-PCR reactions performed with total RNA from infiltrated tobacco leaves or transformed Arabidopsis plants were successful. Unexpectedly, in all cDNAs analyzed the first predicted *AtINT3* intron was spliced incorrectly, i.e. 95 bp from the 3′ end of the first predicted exon were removed together with the first intron, and in none of the analyzed sequences the second intron was spliced out.

The obtained *AtINT3* cDNAs were 1,742 bp long and carried a stop codon after the first 546 bp. This open reading frame (ORF) encodes a truncated protein with 182 amino acids. Only the first 148 amino acids (covering four of the predicted 12 transmembrane helices of AtINT3) corresponded to the predicted AtINT3 protein sequence. Amino acids 149 to 182 resulted from a frameshift due to the incorrect splicing. The obtained cDNA sequence was deposited in the EMBL database (accession no. AM778029).

Obviously, neither in tobacco nor in Arabidopsis the genomic *AtINT3* sequence is spliced as predicted, indicating that *AtINT3* is most likely not a functional gene. Therefore, additional expression analyses in yeast and studies of the activity of the *AtINT3* promoter were not performed.

The *AtINT2* ORF (*At1g30220*) encodes a protein of 580 amino acids, with two consensus sequences for *N*-glycosylation (Asn_{310} and Asn_{382}) and 12 predicted transmembrane helices (Schneider et al., 2006). Figure 1 presents a phylogenetic tree that is based on the experimentally confirmed protein sequences of AtINT1, AtINT2, and AtINT4 (Schneider et al., 2006), on the predicted sequence of AtINT3, on three confirmed or predicted inositol transporter sequences from ice plant (MITR1, MITR2, and MITR3; Chauhan et al., 2000), and on nine homologous sequences found in publicly accessible data libraries (five from rice [*Oryza sativa*], three from *Medicago truncatula*, and one from pineapple [*Ananas comosus*]). The tree falls into three separate clades (1–3 in Fig. 1) and members of the Arabidopsis family and rice sequences are found in each clade. Interestingly, all members of clades 2 and 3 possess an enlarged loop between the predicted transmembrane helices IX and X with two conserved Cys-X-X-Cys motifs. Neither the enlarged loop nor the conserved motifs are found in any of the proteins of clade 1.

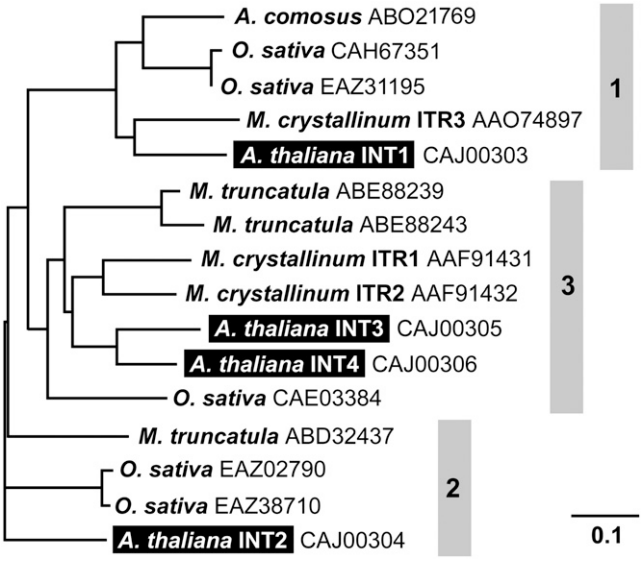

Figure 1. Phylogenetic tree of the AtINT proteins from Arabidopsis and of related proteins from other plant species. Predicted (AtINT3) and confirmed (AtINT1, AtINT2, AtINT4) amino acid sequences of the four Arabidopsis AtINTs plus sequences of 12 homologous proteins from pineapple, rice, *M. truncatula*, and ice plant were aligned (ClustalX; Thompson et al., 1997) and a tree was calculated (TreeViewX; Page, 1996). Protein names (if available) and accession numbers are given.

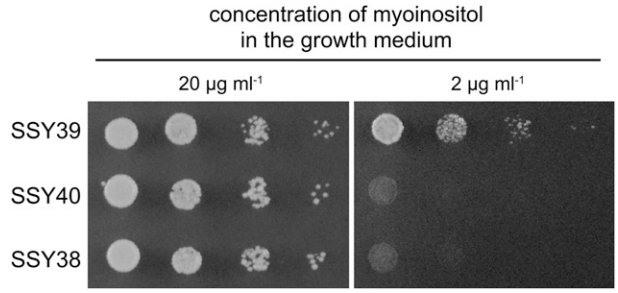

Figure 2. Complementation of the growth defect of D458-1B. Growth of yeast strains SSY39 (=D458-1B with *AtINT2* cDNA in sense), SSY40 (=D458-1B with *AtINT2* cDNA in antisense), and SSY38 (=D458-1B with the empty vector) was analyzed on petri plates (minimal medium) supplemented with the indicated concentrations of myoinositol. While all three strains were able to grow on high myoinositol (20 μg mL^{-1}), only the *AtINT2*-expressing strain was able to grow on low myoinositol (2 μg mL^{-1}).

Expression of the AtINT2 cDNA in Yeast

In a first approach we tried to determine the functional properties of AtINT2 in the bakers' yeast mutant D458-1B (Nikawa et al., 1991). This strain carries mutations in the *ITR1* (inositol transporter) and *INO1* (inositol-1-P synthase) genes and can grow only on high extracellular concentrations of myoinositol. To this end, we cloned the *AtINT2* cDNA into the unique *Not*I site of the yeast expression vector NEV-N-Leu. The resulting plasmids harbored the *AtINT2* cDNA in sense (pSS51s) or antisense orientation (pSS51as).

The transformed yeast lines SSY38 (carrying the empty NEV-N-Leu vector), SSY39 (carrying the *AtINT2* sense plasmid pSS51s), and SSY40 (antisense *AtINT2*) were grown on petri plates containing low (2 μg/mL) or high concentrations (20 μg/mL) of myoinositol to visualize a possible complementation of the described mutations. Figure 2 shows that SSY39 cells had, in fact, regained the capacity to grow on low myoinositol. As expected, no growth was seen for the control strains SSY38 and SSY40 on the same medium. After this initial evidence that *AtINT2* might encode a myoinositol transporter, we tried to characterize the functional and kinetic properties in detail by transport analyses with ^{3}H-labeled myoinositol in SSY39 cells. However, the uptake rates were too low to yield statistically solid data (data not shown). This suggested that the amount of AtINT2 protein in yeast plasma membranes was sufficient for complementation, but not high enough to allow direct measurements of radiolabeled substrates.

Expression of the *AtINT2* cDNA in *Xenopus laevis* Oocytes

Xenopus laevis oocytes have been used for the successful expression of *AtINT4* (Schneider et al., 2006) and for analyses of several other electrogenic plant plasma membrane transporters (Aoshima et al., 1993; Boorer et al., 1996; Klepek et al., 2005; Reinders et al., 2005). As the yeast complementation data suggested plasma membrane localization also for AtINT2, we decided to analyze AtINT2 in this expression system. To this end, the *AtINT2* cDNA was cloned into pDK148 (Jespersen et al., 2002) yielding pSS52s. cRNA was transcribed from the T7 promoter of pSS52s and injected into oocytes that were analyzed for inward currents resulting from the cotransport of cations with potential substrates.

Figure 3A shows a typical recording of inward currents in the presence of various candidate substrates. Analyses were performed with 20-mM solutions of myoinositol, xylitol, mannitol, sorbitol, Glc, Fru, and Suc at an extracellular pH of 5.5. Only application of myoinositol resulted in strong inward currents. Much weaker currents (<10% of myoinositol) were elicited by Glc; no currents were obtained with any of the other compounds (quantitative analyses are shown in Fig. 4A). This demonstrated that, as predicted from the analyses in yeast, AtINT2 does mediate the uptake of myoinositol. Furthermore, the obtained currents confirmed that AtINT2-driven transport is energy dependent, they suggested that a positive charge is likely to be symported with myoinositol, and they demonstrated that AtINT2 is quite specific and does not or hardly transport linear polyols, mono-, or disaccharides.

Myoinositol represents only one of nine possible inositol epimers. Seven of these epimers (allo-, D-chiro-, L-chiro-, muco-, myo-, neo-, and scylloinositol) are found in living cells, the others (cis- and epiinositol) possibly exist only as synthetically prepared compounds. Especially D-chiroinositol (altered orientation of the OH group at position 1 of myoinositol) and scylloinositol (altered orientation of the OH group at position 2 of myoinositol) were also found in plant phospholipids (Chien et al., 1996; Narasimhan et al., 1997; Carstensen et al., 1999). We compared the ability of AtINT2 to transport different epimers of inositol, including the frequently found epimers myo-, D-chiro-, and scylloinositol and two epimers that were not or hardly detected in plant cells (alloinositol [altered orientation of the OH group at position 6 of myoinositol] and mucoinositol [altered orientations of the OH groups at positions 1 and 6 of myoinositol]). Figures 3B (original recording) and 4B (quantitative analysis) demonstrate that in addition to the already shown transport of myoinositol (Figs. 3A and 4A) AtINT2 does also catalyze the transport of scyllo- and D-chiroinositol with only slightly reduced rates (90% and 70%, respectively). Lower current amplitudes (35% and 10%) were obtained in the presence of muco- and alloinositol. We also analyzed the myoinositol derivatives pinitol (monomethylated chiroinositol), phytate (6-fold phosphorylated), and galactinol (inositol attached to Gal). While pinitol was transported by AtINT2 (20% of the rate of myoinositol), no

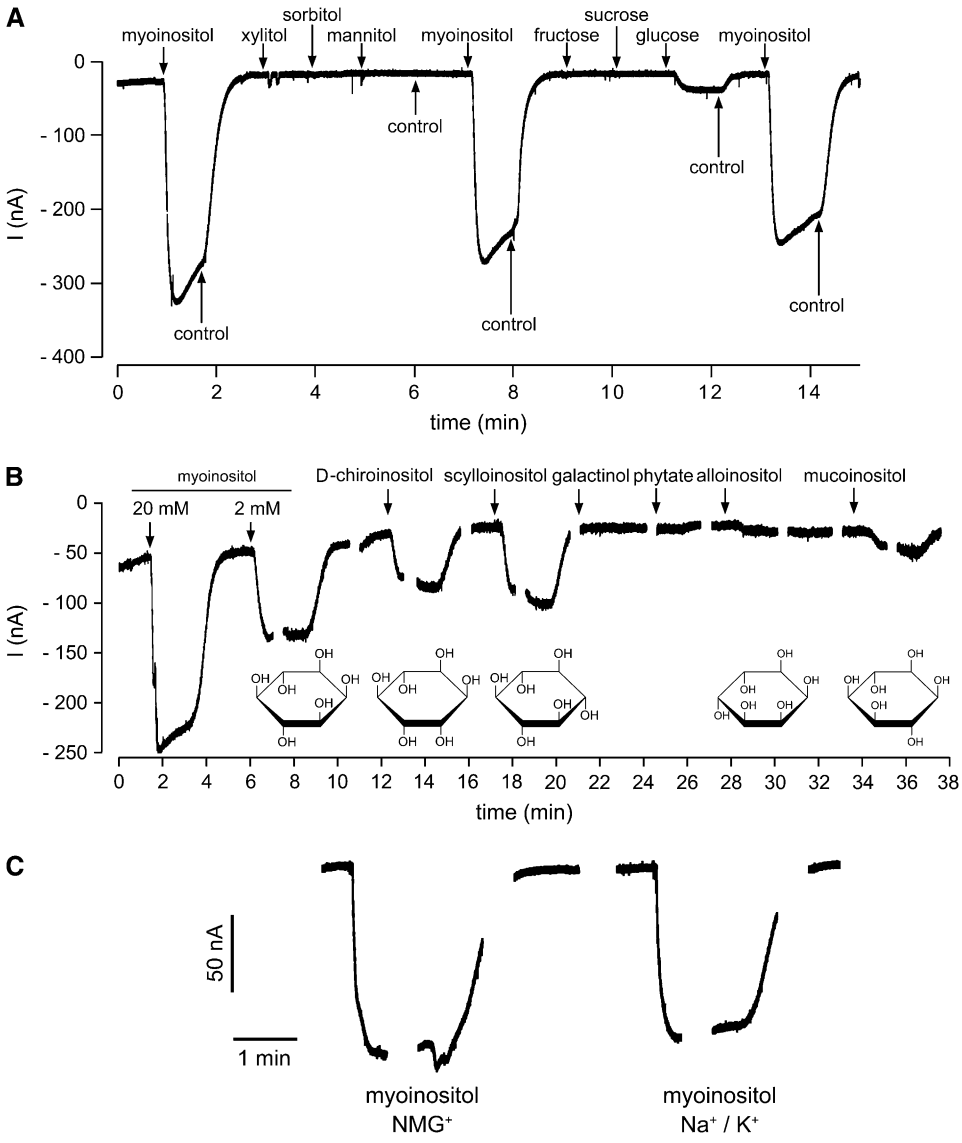

Figure 3. Substrate-induced currents of *AtINT2*-expressing *Xenopus* oocytes. A, AtINT2 mediates inward currents in response to myoinositol but not to most of the other sugars or sugar alcohols tested (all concentrations were 20 mM). Currents were recorded continuously at pH 5.5 and a membrane potential of −60 mV. B, AtINT2-dependent inward currents elicited by different inositol epimers and derivatives. Currents were continuously recorded at pH 5.5 and a membrane potential of −60 mV, gaps result from voltage pulses applied during these times. Structural formulas of inositol epimers are shown underneath the respective recordings. C, Substrate-induced currents do not result from inward Na^+ or K^+ currents. Myoinositol-induced currents were recorded in the presence of 112.5 mM *N*-methylglucamine chloride (left) or 2.5 mM KCl and 110 mM NaCl (right) in the bath solution.

currents were elicited by phytate and galactinol (Figs. 3B and 4B).

The epimer specificity has so far neither been determined for the previously characterized AtINT4 transporter (Schneider et al., 2006) nor for any other plant myoinositol transporter. To observe possible differences in the substrate specificities of AtINT2 and AtINT4 we studied the transport of different inositol epimers also in *Xenopus* oocytes injected with *AtINT4* cRNA. The insert in Figure 4B demonstrates that AtINT2 and AtINT4 show, in fact, clearly different specificities.

The identity of the cotransported ion was determined in the presence of different cations in the extracellular solution. There was no difference between the substrate-induced currents elicited in a buffer containing 110 mM NaCl and 2.5 mM KCl or in a buffer that replaced these salts by *N*-methylglucamine chloride (112.5 mM; Fig. 3C; $n = 6$). This demonstrates that neither K^+ nor Na^+ ions are symported, and that AtINT2 is most likely an inositol/H^+ symporter.

Figure 4C shows the pH dependence of inward H^+ currents elicited by myoinositol in *AtINT2*-expressing *Xenopus* oocytes. AtINT2 shows highest transport rates at physiological and acidic pH values. At more alkaline values, myoinositol-induced currents decrease rapidly, which can be taken as additional, though circumstantial evidence that protons are the cosubstrate of AtINT2.

Finally, the K_m value of AtINT2 was determined for myoinositol. Figure 4D shows Michaelis-Menten kinetics determined at a membrane potential ($\Delta\psi$) of −60 mV and at an extracellular pH of 5.5. Comparison of the K_m value calculated from this and similar analyses at different membrane potentials (insert in Fig. 4D) revealed that the K_m of AtINT2 is slightly

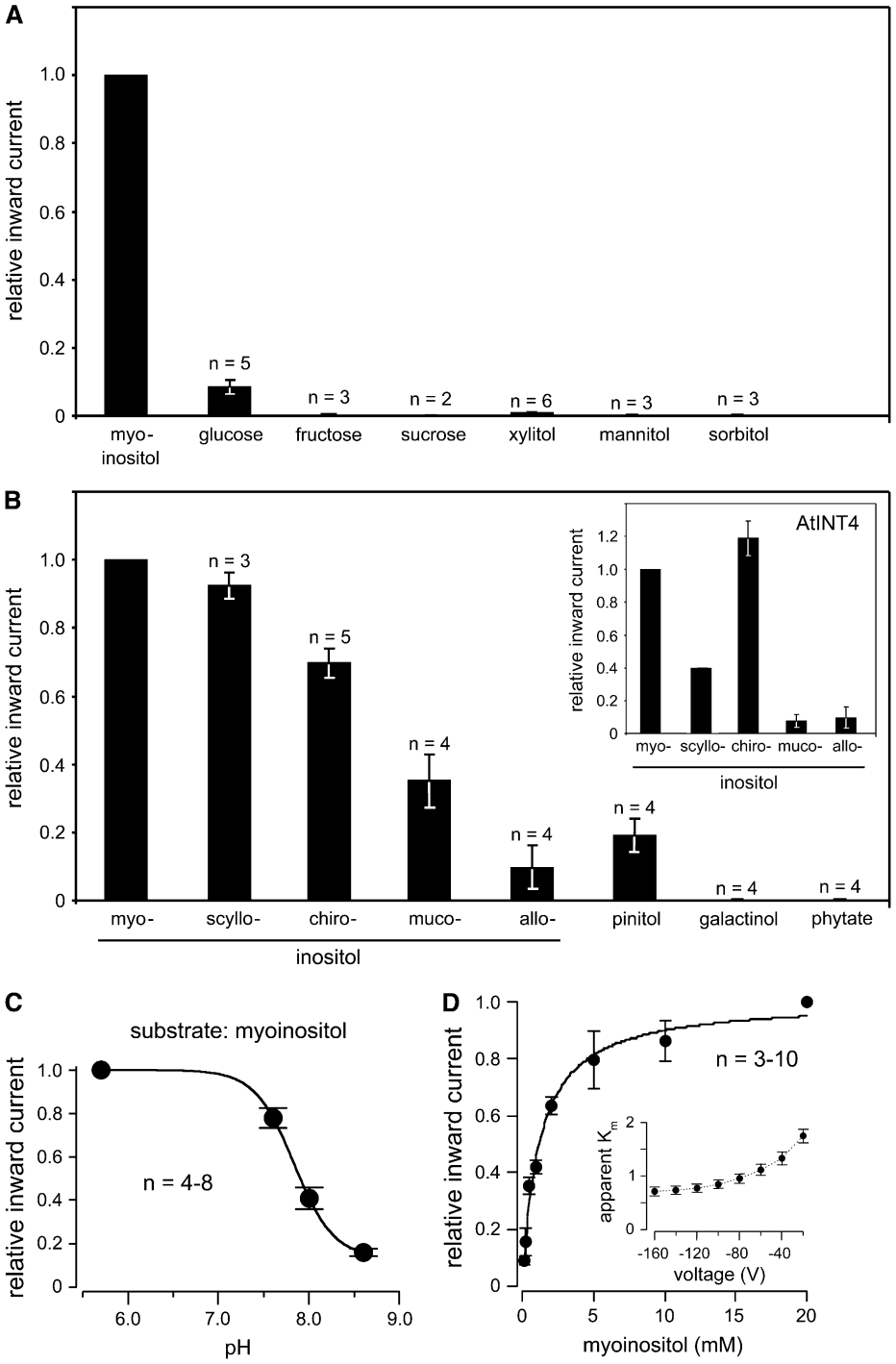

Figure 4. Quantitative analyses of the substrate specificity, pH dependence, and K_m myoinositol of recombinant AtINT2 in *Xenopus* oocytes. A, Quantitative analysis of inward currents elicited by different potential substrates of AtINT2 showing high specificity for inositol and a marginal capacity to transport Glc. B, Relative inward currents elicited by different inositol epimers and derivatives in *AtINT2*-expressing or *AtINT4*-expressing (inset) oocytes. C, pH dependence of myoinositol-elicited inward currents. D, The K_m value of AtINT2 for myoinositol was determined by analyzing H^+ currents in the presence of different myoinositol concentrations. Normalized currents were plotted against the substrate concentration. Data were fitted with Michaelis-Menten-type kinetics. The voltage dependence of the K_m values is shown in the inset. Apparent K_m values ranged from 0.7 ± 0.08 at −160 mV to 1.75 ± 0.13 at −20 mV (n = 5). Myoinositol-dependent H^+ currents were determined at a membrane potential of −60 mV (A–D) or at voltages indicated (inset in D). Results ± SE are presented.

voltage dependent (higher membrane potentials resulted in higher substrate affinity). However, a stronger decrease in the affinity of AtINT2 for myoinositol was observed only at unphysiologically low values of $\Delta\psi$. At −80 mV, a K_m of 0.95 ± 0.09 mM (SE; n = 5) could be determined. This K_m is significantly lower than that determined for AtPLT5 in *Xenopus* oocytes (3.5 ± 0.3 mM; Klepek et al., 2005), but about 4-fold higher than the K_m for myoinositol of AtINT4 (0.24 ± 0.01; Schneider et al., 2006), indicating that AtINT2 is an inositol transporter with medium affinity.

Analysis of *AtINT2* Expression in *AtINT2* Promoter/*GUS* Plants and in *AtINT2* Promoter/*GFP* Plants

For analyses of the tissue specificity of *AtINT2* expression we generated and analyzed *AtINT2* promoter/*GUS* plants and *AtINT2* promoter/*GFP* plants.

To this end a 1,448-bp promoter fragment was used to drive expression of *GUS* or *GFP* in plants that had been selected for BASTA resistance after transformation with the plasmids pLEX111 (=*AtINT2* promoter/*GUS*) or pLEX106 (=*AtINT2* promoter/*GFP*).

We obtained numerous transformants with both constructs and analyzed 30 independent *AtINT2* promoter/*GUS* lines and 24 independent *AtINT2* promoter-*GFP* lines. In none of the *AtINT2* promoter/*GFP* lines we were able to detect GFP fluorescence, suggesting that the activity of the *AtINT2* promoter is rather weak. This was confirmed by analyses of *AtINT2* promoter/*GUS* plants. Although all plants showed the same tissue specificity of the *AtINT2* promoter, the obtained GUS staining was weak and in many plants it was detected only after prolonged staining. The results are summarized in Figure 5. Strongest GUS staining was detected in anthers (Fig. 5A). Analyses at higher magnification (Fig. 5B) and in destroyed anther tissue (Fig. 5C) revealed that this anther-specific GUS staining is not localized in pollen, but rather in a cell layer of the anther wall, most likely the tapetum. This is deduced from two observations: (1) the outermost cell layer of intact anthers shown in Figure 5B were not stained, and (2) individual pollen grains in squashed anther tissue did not show any GUS staining. Interestingly, the previously reported GUS staining in anthers of *AtINT4* promoter/*GUS* plants (Schneider et al., 2006) was pollen specific.

AtINT2 promoter-dependent GUS activity was also seen in Arabidopsis leaves (Fig. 5D) and very weakly in roots (data not shown). Clearly, stronger staining was obtained in leaf vascular tissue of *AtINT2* promoter-*GUS* plants, however, staining was also seen in all other parts of the leaves.

Immunohistochemical Analyses of AtINT2 Localization

Antisera were raised in one guinea pig and two rabbits against a 26-amino acid peptide from the very C terminus of AtINT2. This sequence is not found in any other Arabidopsis protein and does not show significant homology to the C termini of the other AtINT proteins. The quality of the obtained sera was tested on detergent extracts from total membranes isolated from yeast strains ScLEX41 (SEY2102 [Emr et al., 1983] that harbors the NEV-N vector [Sauer and Stolz, 2000] with *AtINT2* cDNA in sense orientation) and SSY9 (SEY2102 that harbors the empty NEV-N vector). Figure 6A shows a western-blot of these extracts after electrophoretic separation and incubation with the unpurified guinea pig antiserum (αAtINT2-GP; similar results were obtained with the rabbit-derived antisera). A band with an apparent molecular mass of about 55 kD was detected only in extracts from *AtINT2*-expressing cells. This band was absent from extracts from SSY9 control cells showing that the labeled band in ScLEX41 cells represents the AtINT2 protein.

The difference between the apparent molecular mass (55 kD) and the molecular mass predicted from the DNA sequence (63.4 kD) was not unexpected. Typically, lipophilic proteins run at lower apparent molecular masses on SDS gels. This unusual running behavior results from excess binding of SDS of highly

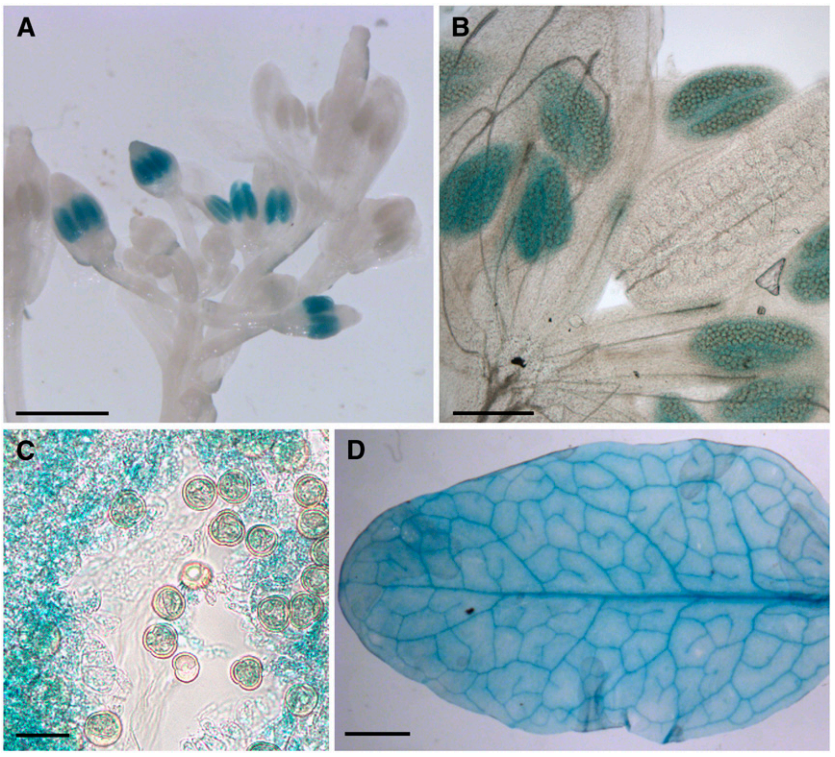

Figure 5. Analysis of *AtINT2* promoter/*GUS* plants. A, GUS histochemical staining of an inflorescence showing GUS staining only in anthers. Notably GUS staining is missing from very young and from fully developed anthers. B, A higher magnification of one of the developing flowers shown in A, suggesting that GUS staining is not in the pollen, but rather in the surrounding tissue, potentially in the tapetum. C, Squashed, GUS-stained anther confirming that the GUS activity is absent from the pollen grains. D, GUS histochemical staining in the vascular strands of a rosette leaf. Weaker staining is seen all over the leaf. Bars are 20 μm in C, 100 μm in B, 1 mm in A, and 2 mm in D.

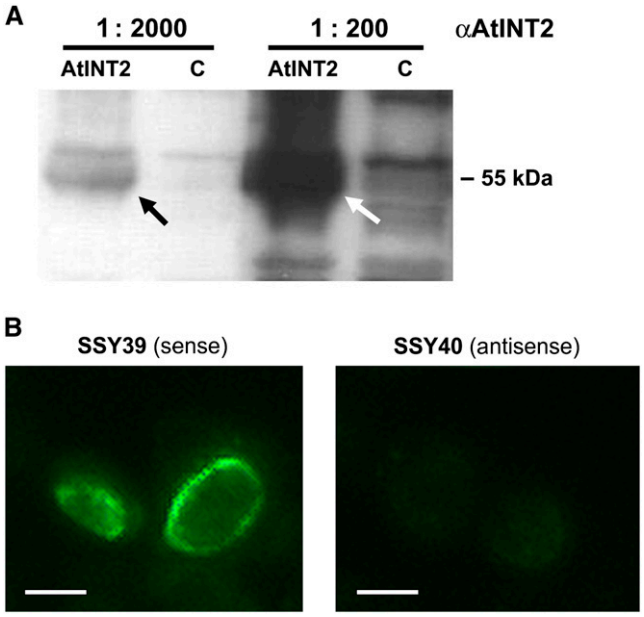

Figure 6. Immunohistochemical detection of recombinant AtINT2 protein in western blots of yeast total membranes and in thin sections of *AtINT2*-expressing yeast cells. A, Unpurified αAtINT2 (diluted 1:200 or 1:2,000) that had been raised against 26 amino acids from the AtINT2 C terminus labeled a 55-kD band in detergent extracts from yeast total membranes after gel electrophoresis and blotting to nitrocellulose filters (10 μg lane^{-1}; AtINT2 = *AtINT2*-expressing cells; C = control cells). B, Incubation of thin sections with affinity-purified αAtINT2 and fluorescence-tagged second antibody yielded fluorescence only in *AtINT2*-expressing cells (SSY39) but not in control cells (SSY40). Bars are 2 μm. [See online article for color version of this figure.]

lipophilic proteins (Beyreuther et al., 1980; Gahrtz et al., 1994; Barth et al., 2003; Schneider et al., 2006).

Next we tested the quality of the antisera on thin sections of yeast cells that expressed *AtINT2* either in sense (SSY39) or in antisense orientation (SSY40; see above). Sections of these cells were prepared using the identical protocol usually applied for the fixation and embedding of plant material (Meyer et al., 2004). Figure 6B demonstrates that affinity-purified αAtINT2-R2 antiserum (from rabbit 2) does recognize the AtINT2 protein in sections of SSY39 cells (sense), but not in SSY40 cells (antisense). This result demonstrated that the antigenic epitope recognized by αAtINT2-R2 was not destroyed during fixation and suggested that αAtINT2-R2 should also detect AtINT2 in plant tissue sections.

Therefore, affinity-purified αAtINT2-R2 was used to study the localization of AtINT2 protein in sections of Arabidopsis leaves and flowers. Antibody binding was visualized with an anti-rabbit IgG-fluorescein isothiocyanate-isomer 1 conjugate. Unfortunately, in none of the tested Arabidopsis tissues αAtINT2-R2-dependent fluorescence was detected. Based on the data from *AtINT2*-expressing yeast cells (Fig. 6B) we could exclude that this results from a destruction of the antigenic epitope during fixation and/or embedding. The complete lack of immunosignals in plant sections rather suggested that the concentration of the antigen is too low for immunodetection of AtINT2 with our antisera. This interpretation was supported by the lack of GFP fluorescence in *AtINT2* promoter/*GFP* plants and by the observed weak GUS histochemical staining.

Analysis of the Subcellular Localization of AtINT2 by Transient Expression of *AtINT2-GFP*

The subcellular localization of AtINT2 in planta was analyzed using an AtINT2 protein with GFP fused to its C terminus. To this end, the plasmid pMG002 that drives expression of the *AtINT2-GFP* fusion under the control of an enhanced *35S* promoter was used for transient expression in Arabidopsis protoplasts (Figs. 7A) or in particle bombarded epidermis cells of Arabidopsis (Fig. 7B) or tobacco (Fig. 7C). Transformed cells and protoplasts were analyzed by confocal microscopy. In all analyses the red autofluorescence of the chloroplasts was localized inside the GFP-labeled structure (arrows in Fig. 7). No GFP fluorescence was found in any other structure inside the transformed cells, indicating that in both plant expression systems (Arabidopsis and tobacco) the AtINT2-GFP fusion protein is located in the plasma membrane.

Analysis of an *Atint2* Mutant Line

Screening of publicly accessible libraries identified a mutant line (GARLIC_1264A7 = *Atint2.1*) with a T-DNA insertion in the second intron of the *AtINT2* gene, 644 bp after the start ATG (Fig. 8A). We performed PCR reactions to identify homozygous *Atint2.1* plants (e.g. plant 2 in the PCR shown in Fig. 8A) and used these plants for further analyses. Homozygous mutant plants showed a complete loss of intact *AtINT2* mRNA (1,742-bp band in Fig. 8B). Partial *AtINT2* mRNAs, however, representing sequences flanking the T-DNA insertion could be amplified also from *Atint2.1* RNA preparations. The 197-bp fragment (N in Fig. 8B) flanking the predicted right border of the T-DNA insertion (RB in Fig. 8A) is likely to result from *AtINT2* promoter activity. The 240-bp fragment (C in Fig. 8B) flanking the identified left border (Fig. 8A) of the T-DNA insertion most likely results from promoter activity within the T-DNA insertion. Growth analyses of homozygous *Atint2.1* plants under standard conditions (on soil in the growth chamber: 21°C, 60% relative humidity, long day [16 h light/8 h dark] or short day [8 h light/16 h dark]), on different concentrations of NaCl (10–100 mM), in the presence of mannitol, or on different concentrations of myoinositol in the growth medium (0–100 mM) revealed no visible or metabolic (e.g. altered sugar, polyol, or cyclitol concentrations; data not shown) differences between the T-DNA insertion line and the isogenic wild type. Also the fertility of the plants was not affected by the T-DNA insertion in *AtINT2*.

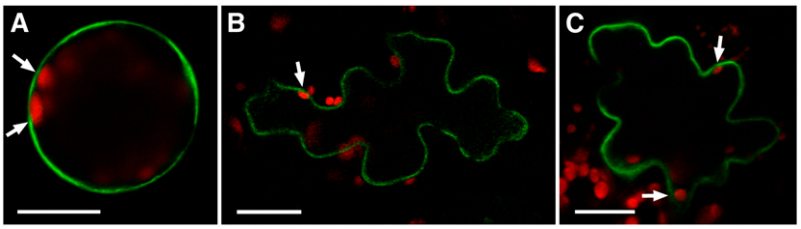

Figure 7. Subcellular localization of AtINT2 in *AtINT2-GFP*-expressing cells. A, Single optical section of an Arabidopsis protoplast. B, Single optical section from an Arabidopsis epidermis cell after particle bombardment of a detached leaf. C, Transient expression in a tobacco epidermis cell after particle bombardment of a detached tobacco leaf. Images were taken on a confocal laser-scanning microscope; red fluorescence in A to C shows chlorophyll autofluorescence. Arrows show localization of chloroplasts inside the GFP-labeled structure. Scale bars are 20 μm.

Analysis of an *Atint2.1*/*Atint4.2* Double Mutant

A possible reason for the lack of a detectable phenotype in the *Atint2.1* mutant might be a functional complementation of the defective *Atint2.1* allele by *AtINT4*. *AtINT4* promoter/*GUS* and *AtINT4* promoter/*GFP* analyses (Schneider et al., 2006) and the *AtINT2* promoter/*GUS* data presented in Figure 6 showed a partial overlap of *AtINT2* and *AtINT4* expression patterns in the vasculature. Therefore, we crossed the *Atint2.1* mutant and the previously described *Atint4.2* mutant (Schneider et al., 2006).

For the identification of *Atint2.1*/*Atint4.2* double mutants, comparative PCRs were performed with genomic DNA isolated from Columbia-0 (Col-0) plants or from potential double mutants and a set of three primers that allowed simultaneous amplification of fragments from wild-type and mutant alleles in a single PCR reaction. Figure 8C shows the characterization of a homozygous *Atint2.1*/*Atint4.2* double mutant that yielded only PCR fragments of the two mutant alleles. These fragments were not amplified from Col-0 DNA that showed the expected wild-type fragments for both genes. Like the *Atint2.1* single

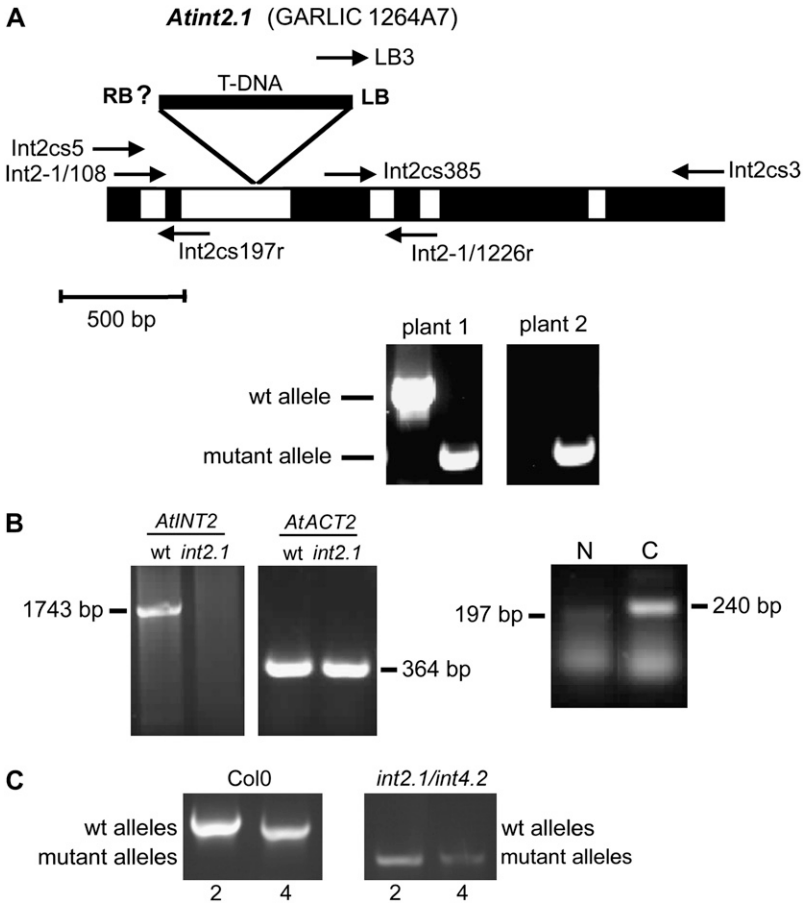

Figure 8. Characterization of GARLIC line 1264A7 (=*Atint2.1*). A, Schematic drawing of the *AtINT2* genomic sequence from start to stop. Exons are shown in black, the five introns in white. The position of the T-DNA insertion and of the characterized left border (LB) are indicated. Arrows show the positions and directions of primers used for PCR reactions in A and B. Example PCRs for two progeny plants of GARLIC_1264A7 seeds identifying wild-type (primers: Int2-1/108 and Int2-1/1226r) and mutant (primers: LB3 and Int2-1/1226r) alleles are presented. Plant 1 was characterized as heterozygous, plant 2 as homozygous. B, RT-PCR-derived bands showing the complete *AtINT2* ORF (primers: Int2cs5 and Int2cs3) and the partial *AtACT2* ORF (primers: ACT2-846f and ACT2-1295r) from RNA isolated from wild-type or Atint2.1 plants. While an *AtINT2* product was obtained only from wild-type plants, the *ACT2* fragment was amplified both from wild-type and mutant plants. cDNA fragments were amplified from truncated mRNAs upstream and downstream of the insertion site (N: primers Int2cs5 and Int2cs197r; C: primers Int2cs385 and Int2-1/1226r). C, Characterization of an *Atint2.1/Atint4.2* double mutant. Only in Col-0 but not in the double mutant the wild-type alleles of *AtINT2* and *AtINT4* were identified (primers: Int2-1/108 and Int2-1/1226r for *AtINT2*; int4-802 and int4-1826r for *AtINT4*; Schneider et al. [2006]). In contrast, mutant alleles were amplified only in the double mutant (primers: LB3 and Int2-1/1226r for *Atint2.1*; int4-802 and LBb1 for *Atint4.2*; Schneider et al. [2006]).

mutant, the *Atint2.1*/*Atint4.2* double mutant neither developed a growth phenotype under different growth conditions nor did we observe differences in the carbohydrate compositions of leaf extracts (myoinositol, Glc, Fru, Suc; data not shown).

DISCUSSION

This article presents a detailed characterization of AtINT2 as a plasma membrane-localized H^+ symporter with medium affinity for various inositol epimers, and of *AtINT3* as a gene that very likely encodes a truncated protein. *AtINT2* and *AtINT3* represent two of four predicted inositol transporter genes (*AtINT1* to *AtINT4*) that form a subfamily within the *MST*-like superfamily of Arabidopsis that was named after the *AtSTP* family of plasma membrane-localized monosaccharide transporters (Sauer et al., 1990; Büttner and Sauer, 2000; Büttner, 2007).

So far, less than 50% of the members of the *MST*-like superfamily (53 genes in Arabidopsis) have been characterized on a functional basis. This includes most members of the *STP* subfamily (Büttner, 2007), one member of the *PLT* subfamily (AtPLT5; Klepek et al., 2005), one member of the *TMT* subfamily of tonoplast-localized monosaccharide transporters (AtTMT1; Wormit et al., 2006), one member of the *VGT* subfamily of vacuolar Glc transporters (AtVGT1; Aluri and Büttner, 2007), and one member of the *AtINT* subfamily (AtINT4; Schneider et al., 2006). Individual members of other subfamilies were studied (AtERD6 [At1g08930], Kiyosue et al., 1998; pGlcT [At5g16150], Weber et al., 2000; AtSFP1 [At5g27350], Quirino et al., 2001), but not functionally characterized.

AtINT3 Seems to Be a Pseudogene

Our attempts to obtain an *AtINT3* cDNA via RT-PCR from total RNA from Arabidopsis rosettes failed repeatedly. Moreover, publicly accessible libraries did not contain *AtINT3* cDNA clones. Finally, no correctly spliced *AtINT3* cDNAs could be isolated from plant tissues (Arabidopsis or tobacco) that expressed genomic *AtINT3* sequences under the control of the *35S* promoter. All obtained cDNAs were incorrectly spliced and encoded only a truncated protein. As can be seen from the phylogenetic tree shown in Figure 1, AtINT3 is closely related to AtINT4, suggesting that the corresponding genes may have duplicated in the more recent past of Arabidopsis evolution. Obviously one of the duplicated genes, *AtINT3*, accumulated mutations that eventually caused a loss of function. Similar observations have been reported for members of the Arabidopsis Suc transporter family (Sauer et al., 2004).

AtINT2 Is a Plasma Membrane-Localized H^+ Symporter That Differs in Its Substrate Specificities from AtINT4

The successful functional analyses in yeast (complementation of a defect in the plasma membrane myo-inositol transporter Itr1p) and *Xenopus* suggested that AtINT2 might be a plasma membrane-localized protein in plant cells. This was confirmed by transient expression analyses of an *AtINT2-GFP* construct that resulted in GFP fluorescence exclusively in the plasma membrane of transformed cells (Fig. 7). Moreover, the *Xenopus* data characterized AtINT2 as an H^+/inositol symporter with medium affinity to myoinositol. In contrast to AtINT4 that has a 4-fold lower, $\Delta\psi$-independent K_m for myoinositol (Schneider et al., 2006) the affinity of AtINT2 increases with increasing $\Delta\psi$.

Another difference between AtINT2 and AtINT4 was observed, when the currents elicited by different inositol epimers were compared (Figs. 3B and 4B). At most likely saturating substrate concentrations (20 mM), AtINT2 catalyzed the uptake of myoinositol and scylloinositol with similar rates. D-chiro-, muco-, and alloinositol were also transported, although with decreasing uptake rates. Under identical conditions, however, AtINT4 preferred myoinositol and D-chiroinositol (D-chiroinositol even slightly better), transported scylloinositol with significantly lower rates, and muco- and alloinositol turned out to be only poor substrates for AtINT4. This demonstrates that AtINT2 and AtINT4 respond differently to altered orientations of the OH groups at position 1 of myoinositol (as in chiroinositol; best substrate for AtINT4) and position 2 (as in scylloinositol; very good substrate for AtINT2). In contrast, an altered orientation of the OH group at position 6 of myoinositol (as in muco- and alloinositol) resulted in reduced transport by both proteins.

AtINT2 and AtINT4 transported pinitol, the monomethylated derivative of chiroinositol, only with reduced rates (about 20%–30% of chiroinositol; Fig. 4B; Schneider et al., 2006), suggesting that unmethylated inositols are the preferred substrates in Arabidopsis. This is supported by results of Miyazaki et al. (2004) obtained with yeast cells expressing inositol transporter cDNAs from ice plants (named *McITR1* or *MITR1*; Chauhan et al., 2000) or Arabidopsis (named *AtITR1* or *AITR1*; identical to *AtINT4*; Schneider et al., 2006). In these analyses, even a 600-fold excess of ononitol (4-*O*-methyl-myoinositol) inhibited myoinositol uptake only by 75%.

Although data on tissue or cellular concentrations of scyllo- and chiroinositol are not available for Arabidopsis, the finding of these inositol epimers in numerous other plant species (Kinnard et al., 1995; Narasimhan et al., 1997; Ichimura et al., 2000) makes it quite likely that Arabidopsis also contains different inositol epimers, and that AtINT2 and AtINT4 may, in fact, see different potential substrates.

Substrate specificities of inositol transporters have also been studied in several nonplant organisms, and for some of these transport systems they are similar to those described for AtINT2 and AtINT4. For the ciliate *Tetrahymena vorax*, for example, it was found that the most frequently occurring epimers myo-, scyllo-, and D-chiroinositol were transported across the plasma membrane (Kersting and Ryals, 2004). Similarly, it was

shown for human HepG2 liver cells that myoinositol and D-chiroinositol are transported by the same protein (Ostlund et al., 1996). Interestingly, however, in the yeast *Candida albicans* (Jin and Seyfang, 2003) and in the protozoan parasite *Leishmania donovani* (Mongan et al., 2004) transporters were identified that are highly specific for myoinositol, because no or only marginal competition by scyllo- or D-chiroinositol was seen. Moreover, for both inositol transport systems a 50% inhibition of myoinositol transport by phytate was observed. This compound elicited no current in *AtINT2*-expressing *Xenopus* oocytes (Figs. 3B and 4B).

AtINT2 Has a Highly Conserved, Cys-Rich Sequence in a Predicted Extracellular Loop

Analyses of the protein sequences of the (putative) inositol transporters shown in the phylogenetic tree in Figure 1 revealed that the loops between the predicted transmembrane helices IX and X of all transporters in clades 2 and 3 are about 80 amino acids longer than the respective loops of the proteins in clade 1. These additional 80 amino acids possess an unusually large number of highly conserved Cys residues. Four of these residues are part of two Cys-X-X-Cys motifs typically separated by only few amino acids (e.g. 399-CMTCLKASSPSCGYC-413 in AtINT2 and 406-CMKCLRSECGFC-417 in AtINT4). Since AtINT2 and AtINT4 were both localized to the plasma membrane, their Cys-X-X-Cys-containing loops are predicted to face the extracellular space and the lumen of the endoplasmic reticulum during biosynthesis and targeting.

Possibly, these highly conserved Cys residues are substrates for endoplasmic protein disulphide isomerases. Alternatively, the Cys-X-X-Cys motifs may provide some yet uncharacterized function to the extracellular loop or confer special redox sensitivity to the protein. Thioredoxins, for example, and bacterial disulphide isomerases have quite similar Cys-X-X-Cys motifs (Elton et al., 2005) and most of these proteins were shown to catalyze redox reactions.

AtINT2 Is Expressed in Anthers and in the Vasculature

Expression of the *AtINT2* gene was observed in anthers (Fig. 5, A–C), in the vascular tissue (Fig. 5D), and to a lesser extent also in the leaf mesophyll (Fig. 5D). The low intensity of the obtained GUS staining and the lack of GFP fluorescence suggested low expression levels for *AtINT2*, and, in fact, we were not able to immunolocalize AtINT2 protein in plant tissue, although the antiserum was shown to work on western blots (Fig. 6A) and in thin sections of *AtINT2*-expressing yeast cells.

At first sight, the expression patterns of *AtINT2* (Fig. 5) and *AtINT4* (Schneider et al., 2006) look similar. The promoters of both genes are active in anthers and in the vasculature. Detailed comparisons show, however, that the anther-specific activity of the *AtINT2* promoter is restricted to cells of the anther wall, most likely the tapetum, a nutrient-supplying cell layer, whereas the anther-specific activity of the *AtINT4* promoter is restricted to the pollen grains. Moreover, the *AtINT2* promoter is active only during a very limited period of anther development (Fig. 5A), whereas *AtINT4* drives *GUS* expression preferentially in the pollen of fully developed anthers (Schneider et al., 2006). These differences in the expression pattern suggest also different physiological roles for the two transporters and make functional redundancy of AtINT2 and AtINT4 rather unlikely. In contrast to AtINT4, which is likely to mediate inositol import into germinating and growing pollen tubes (Schneider et al., 2006), the function of AtINT2 may involve the release of inositols from the tapetum to the developing pollen. It is known that 6-fold phosphorylated myoinositol, phytate, is a major constituent of pollen grains (1%–5% of dry weight; Loewus, 1990; Raboy, 1990) and AtINT2 may play a role in feeding myoinositol to the developing pollen. Given a sufficient substrate accumulation inside the cells of the tapetum, even under physiological pH gradients a release function for AtINT2 appears likely, as other plasma membrane H^+ symporters work in either direction (Carpaneto et al., 2005).

More detailed analyses of the GUS data from *AtINT2* and *AtINT4* promoter/*GUS* plants revealed also differences in the expression patterns in leaves. Whereas the *AtINT2* promoter is active in the vasculature and to a lesser extent also in all other parts of the leaf (Fig. 5D), the activity of the *AtINT4* promoter is strictly confined to the vasculature.

The Physiological Role of AtINT2 Remains to Be Elucidated

Due to the absence of a phenotypic difference between *Atint2.1* single or *Atint2.1*/*Atint4.2* double mutants and wild-type plants, a more detailed prediction of the physiological role(s) of AtINT2 is difficult. In the vasculature it may be involved in the supply of inositol for galactinol and thus for raffinose biosynthesis. The concentrations of raffinose in Arabidopsis, however, are very low (Haritatos et al., 2000), and a partial or complete lack of raffinose would not be expected to strongly influence the development of Arabidopsis plants. The low activity of the *AtINT2* promoter in all other leaf cells might indicate that the function of AtINT2 in the leaf mesophyll is simply the retrieval of inositols that diffused out of the cells. This has been postulated for numerous other transporters as well, and, in fact, keeping the cell wall concentrations of free polyols, sugars, amino acids, and other potential nitrogen and carbon sources low (cell wall hygiene) is certainly a very effective mechanism to reduce growth and development of extracellular pathogens.

One may speculate that triple mutants that include also a T-DNA insertion in the *AtINT1* gene might provide additional information. However, only re-

cently AtINT1 has been characterized as a tonoplast-localized inositol transporter, and *Atint1* mutants show increased cellular inositol concentrations and reduced root development (S. Schneider and N. Sauer, unpublished data). The construction of an *Atint1/Atint2/Atint4* triple mutant is on the way, however, with the background of the observed *Atint1*-based phenotypic differences additional effects of *Atint2* or *Atint4* mutations will be difficult to identify.

MATERIALS AND METHODS

Strains and Growth Conditions

Arabidopsis (*Arabidopsis thaliana*; Col wild type) plants were grown in growth chambers on potting soil under a 16 h light/8 h dark regime (22°C, 60% relative humidity) or in the greenhouse under ambient conditions. For expression of *AtINT2* cDNAs in yeast (*Saccharomyces cerevisiae*) we used strains D458-1B (Nikawa et al., 1991) or SEY2102 (Emr et al., 1983). *Escherichia coli* DH5α (Hanahan, 1983) was used for all cloning steps, fusion proteins for antisera were made in *E. coli* Rosetta (Novagen). Transformation of Arabidopsis was performed with *Agrobacterium tumefaciens* GV3101 (Holsters et al., 1980).

cDNA Cloning of *AtINT3*

AtINT3 cDNA was amplified from tobacco (*Nicotiana tabacum*) plants infiltrated with Agrobacteria carrying plasmid pPU6 or from Arabidopsis plants stably transformed (Clough and Bent, 1998) with this plasmid. pPU6 is derived from pEARLEYGATE 100 (Earley et al., 2006) and was designed for expression of genomic *AtINT3* sequences (start to stop including two predicted introns) under the control of the *35S* promoter. For pPU6 construction, genomic *AtINT3* DNA was amplified from Arabidopsis (AtINT3g + 1f: 5′-CACCATGGTGGAAGAAGCATCGAAATCAG-3′; AtINT3g + 1926r: 5′-CTAAGGCGTTTCCACTTGATTTTCCTTGGTCG-3′), inserted into pENTR/D-TOPO (Invitrogen), sequenced, and cloned into pEARLEYGATE 100.

After isolation of total RNA (RNeasy plant mini kit; Qiagen) from infiltrated tobacco leaves (24 h after infiltration) or from rosette leaves of BASTA-selected Arabidopsis plants, *AtINT3* cDNA was amplified using the primers AtINT3g + 1f and AtINT3g + 1926r, cloned into pCR-Blunt-II-Topo (Invitrogen), and sequenced.

AtINT2 cDNA Cloning and Constructs for Yeast Expression

PCR-based cloning of the *AtINT2* cDNA was described (Schneider et al., 2006). During this PCR, *Not*I restriction sites were added to both ends of the cDNA. For yeast expression, these sites were cut with *Not*I, and the cDNA was cloned into the yeast expression vector NEV-N-Leu, a modification of the expression vector NEV-N, where the Ura2 selection marker had been replaced by Leu-3 (Sauer and Stolz, 1994). Plasmids containing the *AtINT2* cDNA in sense (pSS51s) or antisense orientation (pSS51as) plus the empty NEV-N-Leu vector were used for transformation (Gietz et al., 1992) of D458-1B, yielding strains SSY39, SSY40, and SSY38, respectively. If not otherwise indicated, uptake experiments with myo-[1,2-^{3}H(N)]-inositol (American Radiolabelled Chemicals Inc.) were performed at a concentration of 1 mM (final specific activity: 0.2 μCi μmol^{-1}) in 50-mM sodium phosphate buffer (pH 5.0) as described (Sauer et al., 1990).

Synthesis and Injection of cRNA and Two-Electrode Voltage Clamp

Oocytes were injected (General Valve Picospritzer III, Parker Hannifin Corp.) with cRNA from *AtINT2* or *AtINT4* or with RNase-free water and stored at 16°C in ND96 solution (96 mM NaCl, 2 mM KCl, 1.8 mM $CaCl_2$, 1 mM $MgCl_2$, 5 mM HEPES, adjusted to pH 7.4 with NaOH) supplemented with 1% penicillin-streptomycin (Sigma) or Barth's solution [88 mM NaCl, 1 mM KCl, 0.33 mM $Ca(NO_3)_2$, 0.41 mM $CaCl_2$, 82 mM $MgCl_2$, 2.4 mM $NaHCO_3$, 10 mM HEPES, adjusted to pH 7.6 with NaOH] supplemented with 0.1% gentamycin (Sigma). Oocyte currents were studied 4 to 6 d after injection with the two-electrode voltage-clamp technique (Hedrich et al., 1995) using a Turbo Tec-10Cx amplifier (NPI electronic GmbH). During two-electrode voltage-clamp measurements, oocytes were constantly superfused with modified Ringer solution (110 mM NaCl, 2.5 mM KCl, 1.8 mM $CaCl_2$, 1 mM $MgCl_2$) at room temperature. The solution was buffered using 10 mM MES (pH 5.5, adjusted with TRIS) or TRIS (pH 7.4, 8.0, and 8.5, adjusted with MES). Sugars and sugar alcohols were added to the indicated concentrations. For continuous whole-cell current recordings, oocytes were clamped at a holding potential of −60 mV. Starting from this holding potential, voltage-step protocols were applied to test potentials ranging from +60 mV up to −160 mV in 20 mV decrements.

AtINT2 Promoter/*GUS* and *AtINT2* Promoter/*GFP* Constructs and Plant Transformation

A 1,448-bp *AtINT2* promoter fragment was PCR amplified from genomic Arabidopsis DNA. The primers (INT2-p5: 5′-ATAACTTTAAGCTTTTTGTTAGAA-3′; INT2-p3: 5′-TCCTCCCTCCATGGTTTTTTGGGTTAAAAGAGTTAGAA-3′) introduced an N-terminal *Hin*dIII and a C-terminal *Nco*I site that were used to clone the fragment in front of the ORF of *GFP* and a transcriptional terminator in a pUC19-based plasmid (pEPS1/pUC19; Imlau et al., 1999). The fragment was sequenced and the *AtINT2* promoter/*GFP*/terminator box was cloned into pGPTV-BAR (Becker et al., 1992) yielding the plasmid pLEX163 that was used for transformation of Arabidopsis (Clough and Bent, 1998). Plasmid pLEX111 (*AtINT2* promoter/*GUS*) was also generated in pGPTV-BAR using the same promoter fragment.

Transient Expression of *AtINT2-GFP*

The *AtINT2* coding sequence was PCR amplified using the primers AtINT2-5-BspH (5′-TCATGAAGGGAGGAATAATACATG-3′) and AtINT2-5-bspH (5′-TCATGACTGCACTCTGGTTTTGTTTCTC-3′). These primers introduced *Bsp*HI sites at the start and at the very end of the *AtINT2* ORF, thereby replacing the stop codon of the original *AtINT2* sequence. This modified *AtINT2* ORF was inserted into the unique *Nco*I cloning site representing the start ATG of the *GFP* ORF in the pSO35e plasmid (Klepek et al., 2005). The continuous ORF was confirmed by sequencing. The resulting plasmid was named pMG002.

pMG002 was used for transient expression of *AtINT2* in Arabidopsis protoplasts (polyethylene glycol transformation; modified after Abel and Theologis, 1994) or in tobacco or Arabidopsis epidermis cells (particle bombardment; Klepek et al., 2005).

Analysis of the T-DNA Insertion Line *Atint2.1*

The T-DNA insertion line *Atint2.1* (GARLIC_1264A7 = SAIL_1264_A07) was identified using the Salk Institute T-DNA Express gene-mapping tool (Alonso et al., 2003). Homozygous plants were identified in PCR reactions on genomic DNA with the primers Int2-1/108 (5′-ATCGGTGGTCTTCTCTTTGGT-3′) and Int2-1/1226r (5′-CCGGGAGTGTAAACATTAAGACA-3′) in combination with the primer LB3 (5′-TAGCATCTGAATTTCATAACCAATCTC-3′) that binds near the left border within the T-DNA insertion.

Primers Int2cs5 (5′-ATATCTCTGCGGCCGCAAAAATGGAGGGAGGAATAATACAT-3′), Int2cs3 (5′-ATATCTCTGCGGCCGCTCATGCACTCTGGTTTTGTTTCTCA-3′), Int2-1/108, and Int2-1/1226r were used for RT-PCRs with total RNA from wild-type and mutant Arabidopsis leaves. Primers AtACT2g + 846f (5′-ATTCAGATGCCCAGAAGTCTTGTT-3′) and AtACT2g + 1295r (5′-GAAACATTTTCTGTGAACGATTCCT-3′) were used to amplify the *AtACT2* mRNA.

Immunohistochemical Techniques and Western-Blot Analyses

For αAtINT2 production, two oligonucleotides were annealed and cloned into the *Eco*RI/*Hin*dIII-digested vector pMAL-c2 (New England Biolabs) yielding pSS11-AK2. The oligonucleotides encoded the C-terminal 26 amino acids of AtINT2. pSS11-AK2 was used to express a fusion of this peptide to the maltose-binding protein in *E. coli* Rosetta (Novagen). Expression of the protein was induced with isopropyl thiogalactoside, solubilized proteins were sepa-

rated on polyacrylamide gels (Laemmli, 1970), bands were excised, and proteins extracted and lyophilized. Antisera were generated by Pineda-Antikörper-Service.

Binding of αAtINT2 to microtome sections was visualized by treatment with anti-rabbit IgG-fluorescein isothiocyanate-isomer 1 conjugate (Sigma-Aldrich). Microscopic slides were mounted in antifading medium (ProLong Antifade kit; Molecular Probes) and viewed under appropriate excitation light.

Protein extracts of total membrane fractions from bakers' yeast were prepared as described (Sauer and Stolz, 2000), separated on polyacrylamide gels (Laemmli, 1970), and transferred to nitrocellulose filters (Dunn, 1986). Filters were treated with anti-rabbit or anti-guinea pig IgG-peroxidase conjugate (diluted 1:4,000) followed by incubation with Lumi-Light western Blotting Substrate (Roche Diagnostics GmbH).

Ion Chromatography

Concentrations of sugars and sugar alcohols were determined with an ICS-3000 system (Dionex) with a gradient pump (ICS-3000 SP), a degaser module, an autosampler (ICS-3000 AS), and a pulsed amperometric detector (ICS-3000 DC). Anionic compounds were separated on a CarboPack MA1 column (4 × 250 mm) connected to a guard column of the same material (4 × 10 mm) and an ATC-1 anion trap column that was placed between the eluent and separation columns to remove anionic contaminants in the eluents. As eluent, 612 mM sodium hydroxide made from purest water (Millipore) and 50% NaOH (Fluka) was used. The column was equilibrated at a flow rate of 0.4 mL min^{-1}. The duration of the run was 60 min. Calibration and quantitative calculation of carbohydrates was performed with the Dionex chromeleon software 6.7.

Microscopy and Detection of GFP Fluorescence

Images of GFP fluorescence were made with an epifluorescence microscope (Zeiss Axioskop, Carl Zeiss Jena GmbH; excitation wavelength 460–500 nm) or with a confocal laser-scanning microscope (Leica TCS SPII, Leica Microsystems). Emitted fluorescence was monitored at detection wavelengths longer than 510 nm. Confocal images were processed using the Leica Confocal Software 2.5 (Leica Microsystems).

GUS plants were analyzed using a stereomicroscope (Leica MZFLIII; Leica Microsystems) or a microscope (Zeiss Axioskop, Carl Zeiss Jena GmbH). Images were processed using analySIS Doku 3.2 Software (Soft Imaging System).

Sequence data from this article can be found in the GenBank/EMBL data libraries under accession number AM778029 for *AtINT3*.

ACKNOWLEDGMENTS

We thank Ruth Stadler for experimental help and Angelika Wolf for growing the Arabidopsis plants. We are grateful to Christoph Korbmacher for the frequent and generous supply with *Xenopus laevis* oocytes.

Received September 13, 2007; accepted September 24, 2007; published October 19, 2007.

LITERATURE CITED

Abel S, Theologis A (1994) Transient transformation of *Arabidopsis* leaf protoplasts: a versatile experimental system to study gene expression. Plant J **5:** 421–427

Alonso JM, Stepanova AN, Leisse TJ, Kim CJ, Chen H, Shinn P, Stevenson DK, Zimmerman J, Barajas P, Cheuk R, et al (2003) Genome-wide insertional mutagenesis of *Arabidopsis thaliana.* Science **301:** 653–657

Aluri S, Büttner M (2007) Identification and functional expression of the *Arabidopsis thaliana* vacuolar glucose transporter 1 and its role in seed germination and flowering. Proc Natl Acad Sci USA **104:** 2537–2542

Aoshima H, Yamada M, Sauer N, Komor E, Schobert C (1993) Heterologous expression of the H^+/hexose cotransporter from *Chlorella* in *Xenopus* oocytes and its characterization with respect to sugar specificity, pH and membrane potential. J Plant Physiol **141:** 293–297

Barth I, Meyer S, Sauer N (2003) PmSUC3: characterization of a SUT2/SUC3-type sucrose transporter from *Plantago major.* Plant Cell **15:** 1375–1385

Becker D, Kemper E, Schell J, Masterson R (1992) New plant binary vectors with selectable markers located proximal to the left T-DNA border. Plant Mol Biol **20:** 1195–1197

Beyreuther K, Bieseler B, Ehring R, Griesser HW, Mieschendahl M, Müller-Hill B, Triesch I (1980) Investigation of structure and function of lactose permease of *Escherichia coli.* Biochem Soc Trans **8:** 675–676

Boorer KJ, Loo DD, Frommer WB, Wright EM (1996) Transport mechanism of the cloned potato H^+/sucrose cotransporter StSUT1. J Biol Chem **271:** 25139–25144

Büttner M (2007) The monosaccharide transporter(-like) gene family in *Arabidopsis.* FEBS Lett **581:** 2318–2324

Büttner M, Sauer N (2000) Monosaccharide transporters in plants: structure, function and physiology. Biochim Biophys Acta **1465:** 263–274

Carpaneto A, Geiger D, Bamberg E, Sauer N, Fromm J, Hedrich R (2005) Phloem-localized, proton-coupled sucrose carrier ZmSUT1 mediates sucrose efflux under control of sucrose gradient and pmf. J Biol Chem **280:** 21437–21443

Carstensen S, Pliska-Matyshak G, Bhuvarahamurthy N, Robbins KM, Murthy PP (1999) Biosynthesis and localization of phosphatidyl-scyllo-inositol in barley aleurone cells. Lipids **34:** 67–73

Chauhan S, Forsthoefel N, Ran Y, Quigley F, Nelson DE, Bohnert HJ (2000) Na^+/*myo*-inositol symporters and Na^+/H^+-antiport in *Mesembryanthemum crystallinum.* Plant J **24:** 511–522

Chien CT, Lin TP, Juo CG, Her GR (1996) Occurance of a novel galactopinitol and its changes with other non-reducing sugars during development of *Leucaena laucocephala* seeds. Plant Cell Physiol **37:** 539–544

Clough SJ, Bent AF (1998) Floral dip: a simplified method for *Agrobacterium*-mediated transformation of *Arabidopsis thaliana.* Plant J **16:** 735–743

Cohen JD, Bandurski RS (1982) Chemistry and physiology of the bound auxins. Annu Rev Plant Physiol **33:** 403–430

Dunn SD (1986) Effects of the modification of transfer buffer composition and the renaturation of proteins in gels on the recognition of proteins on western blots by monoclonal antibodies. Anal Biochem **157:** 144–153

Earley KW, Haag JR, Pontes O, Opper K, Juehne T, Song K, Pikaard CS (2006) Gateway-compatible vectors for plant functional genomics and proteomics. Plant J **45:** 616–629

Elton TC, Holland SJ, Frost LS, Hazes B (2005) F-like type IV secretion systems encode proteins with thioredoxin folds that are putative DsbC homologues. J Bacteriol **187:** 8267–8277

Emr SD, Scheckman R, Flessel MC, Thorner J (1983) An MFα1-SUC2 (σ-factor-invertase) gene fusion for study of protein localisation and gene expression in yeast. Proc Natl Acad Sci USA **80:** 7080–7084

Gahrtz M, Stolz J, Sauer N (1994) A phloem specific sucrose-H^+ symporter from *Plantago major* L. supports the model of apoplastic phloem loading. Plant J **6:** 697–706

Gietz D, Jean WS, Woods RA, Schiestl RH (1992) Improved method for high efficiency transformation of intact yeast cells. Nucleic Acids Res **20:** 1425

Hanahan D (1983) Studies on transformation of *E. coli* with plasmids. J Mol Biol **166:** 557–580

Haritatos E, Ayre BG, Turgeon R (2000) Identification of phloem involved in assimilate loading in leaves by activity of the galactinol synthase promoter. Plant Physiol **123:** 929–937

Hasegawa PM, Bressan RA, Zhu JK, Bohnert H (2000) Plant cellular and molecular responses to high salinity. Annu Rev Plant Physiol Plant Mol Biol **51:** 463–499

Hedrich R, Moran O, Conti F, Busch H, Becker D, Gambale F, Dreyer I, Kuch A, Neuwinger K, Palme K (1995) Inward rectifier potassium channels in plants differ from their animal counterparts in response to voltage and channel modulators. Eur Biophys J **24:** 107–115

Holsters M, Silva B, Van Vliet F, Genetello C, De Block M, Dhaese P, Depicker A, Inze D, Engler G, Villarroel R, et al (1980) The functional organization of the nopaline *Agrobacterium tumefaciens* plasmid pTiC58. Plasmid **3:** 212–230

Ichimura K, Kohata K, Yamaguchi Y, Douzono M, Ikeda H, Koketsu M (2000) Identification of L-inositol and scyllitol and their distribution in various organs in *Chrysanthemum.* Biosci Biotechnol Biochem **64:** 865–868

Imlau A, Truernit E, Sauer N (1999) Cell-to-cell and long-distance trafficking of the green fluorescent protein in the phloem and symplastic unloading of the protein into sink tissues. Plant Cell **11:** 309–322

Jespersen T, Grunnet M, Angelo K, Klaerke DA, Olesen SP (2002) Dual-function vector for protein expression in both mammalian cells and *Xenopus laevis* oocytes. Biotechniques **32:** 536–540

Jin JH, Seyfang A (2003) High-affinity myo-inositol transport in *Candida albicans*: substrate specificity and pharmacology. Microbiology **149:** 3371–3381

Kandler O, Hopf H (1982) Oligosaccharides based on sucrose (sucrosyl oligosaccharides). *In* FA Loewus, W Tanner, eds, Plant Carbohydrates 1. Encyclopedia of Plant Physiology: Plant Carbohydrates I, Intracellular Carbohydrates, New Series, Vol 13 A. Springer-Verlag, Berlin, pp 348–383

Kanter U, Usadel B, Guerineau F, Li Y, Pauly M, Tenhaken R (2005) The inositol oxygenase gene family of *Arabidopsis* is involved in the biosynthesis of nucleotide sugar precursors for cell-wall matrix polysaccharides. Planta **221:** 243–254

Kersting M, Ryals PE (2004) Sodium-dependent transport of [^{3}H](1D)chiro-inositol by *Tetrahymena.* J Eukaryot Microbiol **51:** 307–311

Kinnard RL, Narasimhan B, Pliska-Matyshak G, Murthy PP (1995) Characterization of scyllo-inositol-containing phosphatidylinositol in plant cells. Biochem Biophys Res Commun **210:** 549–555

Kiyosue T, Abe H, Yamaguchi-Shinozaki K, Shinozaki K (1998) ERD6, a cDNA clone for an early dehydration-induced gene of *Arabidopsis*, encodes a putative sugar transporter. Biochim Biophys Acta **1370:** 187–191

Klepek YS, Geiger D, Stadler R, Klebl F, Landouar-Arsivaud L, Lemoine R, Hedrich R, Sauer N (2005) *Arabidopsis* POLYOL TRANSPORTER5, a new member of the monosaccharide transporter-like superfamily, mediates H^+-symport of numerous substrates, including *myo*-inositol, glycerol, and ribose. Plant Cell **17:** 204–218

Laemmli UK (1970) Cleavage of structural proteins during the assembly of the head of bacteriophage T4. Nature **227:** 680–685

Lehle L (1990) Phosphatidyl inositol metabolism and its role in signal transduction in growing plants. Plant Mol Biol **15:** 647–658

Loewus FA (1990) Structure and occurrence of inositols in plants. *In* DJ Morré, WF Boss, FA Loewus, eds, Inositol Metabolism in Plants. Wiley-Liss Inc, New York, pp 1–11

Loewus FA, Murthy PPN (2000) *myo*-Inositol metabolism in plants. Plant Sci **150:** 1–19

Lorence A, Chevone BI, Mendes P, Nessler CL (2004) *myo*-Inositol oxygenase offers a possible entry point into plant ascorbate biosynthesis. Plant Physiol **134:** 1200–1205

Macbeth MR, Schubert HL, VanDemark AP, Lingam AT, Hill CP, Bass BL (2005) Inositol hexakisphosphate is bound in the ADAR2 core and required for RNA editing. Science **309:** 1534–1539

Meyer S, Lauterbach C, Niedermeier M, Barth I, Sjolund RD, Sauer N (2004) Wounding enhances expression of *AtSUC3*, a sucrose transporter from Arabidopsis sieve elements and sink tissues. Plant Physiol **134:** 684–693

Miyazaki S, Rice M, Quigley F, Bohnert HJ (2004) Expression of plant inositol transporters in yeast. Plant Sci **166:** 245–252

Mongan TP, Ganapasam S, Hobbs SB, Seyfang A (2004) Substrate specificity of the *Leishmania donovani* myo-inositol transporter: critical role of inositol C-2, C-3 and C-5 hydroxyl groups. Mol Biochem Parasitol **135:** 133–141

Murakeözy EP, Nagy Z, Duhazé C, Bouchereau A, Tuba Z (2003) Seasonal changes in the levels of compatible osmolytes in three halophytic species of inland saline vegetation in Hungary. J Plant Physiol **160:** 395–401

Narasimhan B, Pliska-Matyshak G, Kinnard R, Carstensen S, Ritter MA, van Weymarn L, Murthy PN (1997) Novel phosphoinositides in barley aleurone cells. Plant Physiol **113:** 1385–1393

Nelson DE, Rammesmayer G, Bohnert HJ (1998) Regulation of cell-specific inositol metabolism and transport in plant salinity tolerance. Plant Cell **10:** 753–764

Nikawa J, Tskugoshi Y, Yamashita S (1991) Isolation and characterization of two distinct *myo*-inositol transporter genes of *Saccharomyces cerevisiae.* J Biol Chem **266:** 11184–11191

Ostlund RE Jr, Seemayer R, Gupta S, Kimmel R, Ostlund EL, Sherman WR (1996) A stereospecific myo-inositol/D-chiro-inositol transporter in HepG2 liver cells. J Biol Chem **271:** 10073–10078

Page RDM (1996) TREEVIEW: an application to display phylogenetic trees on personal computers. Comput Appl Biosci **12:** 357–358

Quirino BF, Reiter WD, Amasino RD (2001) One of two tandem *Arabidopsis* genes homologous to monosaccharide transporters is senescence-associated. Plant Mol Biol **46:** 447–457

Raboy V (1990) Biochemistry and genetics of phytic acid biosynthesis. *In* DJ Morré, WF Boss, FA Loewus, eds, Inositol Metabolism in Plants. Wiley-Liss Inc, New York, pp 55–76

Raboy V (2003) *myo*-Inositol-1,2,3,4,5,6-hexakisphosphate. Phytochemistry **64:** 1033–1043

Reinders A, Panshyshyn JA, Ward JM (2005) Analysis of transport activity of *Arabidopsis* sugar alcohol permease homolog AtPLT5. J Biol Chem **280:** 1594–1602

Sauer N, Friedländer K, Gräml-Wicke U (1990) Primary structure, genomic organization and heterologous expression of a glucose transporter from *Arabidopsis thaliana.* EMBO J **9:** 3045–3050

Sauer N, Ludwig A, Knoblauch A, Rothe P, Gahrtz M, Klebl F (2004) *AtSUC8* and *AtSUC9* encode functional sucrose transporters, but the closely related *AtSUC6* and *AtSUC7* genes encode aberrant proteins in different *Arabidopsis* ecotypes. Plant J **40:** 120–130

Sauer N, Stolz J (1994) SUC1 and SUC2: two sucrose transporters from *Arabidopsis thaliana*; expression and characterization in baker's yeast and identification of the histidine tagged protein. Plant J **6:** 67–77

Sauer N, Stolz J (2000) Expression of foreign transport proteins in yeast. *In* SA Baldwin, ed, Practical Approach Series. Oxford University Press, Oxford, pp 79–105

Schneider S, Schneidereit A, Konrad KR, Hajirezaei M-R, Gramann M, Hedrich R, Sauer N (2006) *Arabidopsis thaliana INOSITOL TRANSPORTER 4* mediates high affinity H^+-transport of myoinositol across the plasma membrane. Plant Physiol **141:** 565–577

Schultz C, Gilson P, Oxley D, Youl J, Bacic A (1998) GPI-anchors on arabinogalactan-proteins: implications for signalling in plants. Trends Plant Sci **3:** 426–431

Sheveleva E, Chmara W, Bohnert HJ, Jensen RG (1997) Increased salt and drought tolerance by D-ononitol production in transgenic *Nicotiana tabacum* L. Plant Physiol **115:** 1211–1219

Shi J, Wang H, Hazebroek J, Ertl DS, Harp T (2005) The maize *low-phytic acid 3* encodes a myo-inositol kinase that plays a role in phytic acid biosynthesis in developing seeds. Plant J **42:** 708–719

Smith AE, Phillips EV (1982) The maize *low-phytic acid 3* encodes a *myo*-inositol kinase that plays a role in phytic acid biosynthesis in developing seeds. Physiol Plant **54:** 31–33

Streeter JG, Lohnes DG, Fioritto RJ (2001) Patterns of pinitol accumulation in soybean plants and relationships to drought tolerance. Plant Cell Environ **24:** 429–438

Tan X, Calderon-Villalobos LIA, Sharon M, Zheng C, Robinson CV, Estelle M, Zheng N (2007) Mechanism of auxin perception by the TIR1 ubiquitin ligase. Nature **446:** 640–645

Thomas JC, Bohnert HJ (1993) Salt stress perception and plant growth regulators in the halophyte *Mesembryanthemum crystallinum.* Plant Physiol **103:** 1299–1304

Thompson JD, Gibson TJ, Plewniak F, Jeanmougin F, Higgins DG (1997) The ClustalX windows interface: flexible strategies for multiple sequence alignment aided by quality analysis tools. Nucleic Acids Res **25:** 4876–4882

Weber A, Servaites JC, Geiger DR, Kofler H, Hille D, Groner F, Hebbeker U, Flügge UI (2000) Identification, purification, and molecular cloning of a putative plastidic glucose translocator. Plant Cell **12:** 787–802

Wormit A, Trentmann O, Feifer I, Lohr C, Tjaden J, Meyer S, Schmidt U, Martinoia E, Neuhaus HE (2006) Molecular identification and physiological characterization of a novel monosaccharide transporter from *Arabidopsis* involved in vacuolar sugar transport. Plant Cell **18:** 3476–3490